EDGE ARTICLE

Check for updates

Transforming colloidal Cs₄PbBr₆ nanocrystals with poly(maleic anhydride-*alt*-1-octadecene) into stable CsPbBr₃ perovskite emitters through intermediate heterostructures†

Dmitry Baranov, [ID] *[a] Gianvito Caputo, [ID][a] Luca Goldoni,[b] Zhiya Dang,[a]
Riccardo Scarfiello,[c] Luca De Trizio, [ID][a] Alberto Portone, [ID][d] Filippo Fabbri,[d]
Andrea Camposeo, [ID][d] Dario Pisignano [ID][de] and Liberato Manna [ID] *[a]

The preparation of strongly emissive CsPbBr₃ perovskite nanocrystals with robust surface passivation is a challenge in the field of lead halide perovskite nanomaterials. We report an approach to prepare polymer-capped CsPbBr₃ perovskite nanocrystals by reacting oleylammonium/oleate-capped Cs₄PbBr₆ nanocrystals with poly(maleic anhydride-*alt*-1-octadecene) (PMAO). PMAO contains succinic anhydride units that are reactive towards the oleylamine species present on the Cs₄PbBr₆ nanocrystals' surface and produces polysuccinamic acid, which, in turn, triggers the Cs₄PbBr₆ to CsPbBr₃ conversion. The transformation occurs through the formation of Cs₄PbBr₆–CsPbBr₃ heterostructures as intermediates, which are captured because of the mild reactivity of PMAO and are investigated by high-resolution electron microscopy. The Cs₄PbBr₆–CsPbBr₃ heterostructures demonstrate a dual emission at cryogenic temperature with an indication of the energy transfer from Cs₄PbBr₆ to CsPbBr₃. The fully-transformed CsPbBr₃ NCs have high photoluminescence quantum yield and enhanced colloidal stability, which we attribute to the adhesion of polysuccinamic acid to the NC surface through its multiple functional groups in place of oleate and alkylammonium ligands. The PMAO-induced transformation of Cs₄PbBr₆ NCs opens up a strategy for the chemical modification of metal halide NCs initially passivated with nucleophilic amines.

Introduction

Nanocrystals (NCs) of cesium lead halides have recently emerged as a class of semiconductor materials promising for light-emitting applications.[1–3] The chemical reactivity of these NCs and the interconversion between the NCs of the two most studied bromides in this class, Cs₄PbBr₆ and CsPbBr₃ perovskite, have been of interest since these NCs were first synthesized in the colloidal form.[4–8] The Cs₄PbBr₆ → CsPbBr₃ conversion, which can be triggered using various reagents (for example, Prussian blue,[9] oleic acid,[10] PbBr₂,[7,11] and water)[12–14] is an interesting approach to prepare emissive CsPbBr₃ NCs. For

example, Yin's group exploited heterogeneous water-mediated CsBr extraction from Cs₄PbBr₆ NCs in hexane as a method for making luminescent CsPbBr₃/SiO₂ or CsPbBr₃/Ta₂O₅ Janus-type heterostructures,[13] and branched CsPbBr₃ dodecapods.[15] Despite several reports on Cs₄PbBr₆ → CsPbBr₃ transformation at the nanoscale, the nanocrystal intermediates of this reaction and the surface passivation and stability of the resulting CsPbBr₃ NCs have not been investigated.

Designing the Cs₄PbBr₆ → CsPbBr₃ NC transformation in such a way that it delivers encapsulated CsPbBr₃ NCs with an enhanced stability is a promising approach for exploiting the Cs₄PbBr₆ NC reactivity, as shown by the above mentioned studies of Yin's group.[13] The use of an organic polymer instead

ᵃNanochemistry Department, Istituto Italiano di Tecnologia, Via Morego 30, 16163 Genova, Italy. E-mail: dmitry.baranov@iit.it; liberato.manna@iit.it

ᵇAnalytical Chemistry Lab, Istituto Italiano di Tecnologia, Via Morego 30, 16163 Genova, Italy

ᶜCNR NANOTEC, Institute of Nanotechnology, c/o Campus Ecotecne, via Monteroni, 73100 Lecce, Italy

ᵈNEST, Istituto Nanoscience-CNR, Piazza S. Silvestro 12, I-56127 Pisa, Italy

ᵉDipartimento di Fisica "Enrico Fermi", Università di Pisa, Largo Bruno Pontecorvo 3, I-56127 Pisa, Italy

† Electronic supplementary information (ESI) available: Experimental details and procedures, EDS-STEM data, ¹H and ¹H–¹³C HSQC NMR spectra and discussion, annotated XRD patterns, PLQY spectra, FTIR and NIR absorbance spectra, tests of PMAO reactivity with powders of bulk Cs₄PbBr₆ and amine-free Cs₄PbBr₆ NCs, stability tests of CsPbBr₃/PMAO NCs, HRTEM images of Cs₄PbBr₆–CsPbBr₃ heterostructures, low-resolution TEM size analysis, PL maps and spectra of Cs₄PbBr₆ NCs at 27 K, and time-resolved PL, micro-PL, and Raman spectra for the NC-PMAO blend (PDF). A video showing transformation of non-luminescent Cs₄PbBr₆ NCs into green-emitting CsPbBr₃ NCs after addition of PMAO (MP4). See DOI: 10.1039/d0sc00738b.

of an inorganic oxide (*e.g.* SiO_2 or Ta_2O_5) shell would yield a NC-polymer blend which can be drop-cast, spin-coated or electro-spun, widening the range of available applications.[16] More generally, polymer encapsulation of $CsPbX_3$ perovskite NCs (X = Cl, Br, I, and their mixtures) is promising because it has been shown to enhance the shelf-time of NCs by providing enhanced stability against moisture and photodegradation.[17] Interestingly, stability enhancement has been reported irrespective of whether polymer chains preserve the native $CsPbX_3$ NC surface ligands as in the case of polystyrene[17–19] and poly(styrene–ethylene–butylene–styrene),[17] or whether the polymer adheres to the surface of $CsPbX_3$ NCs as in the case of ammonium bromide-terminated polystyrene[20] or poly(*n*-butyl methacrylate) modified with zwitterionic sulfobetaine or phosphorylcholine functional groups.[21] Arguably, an ideal NC transformation of $Cs_4PbBr_6 \rightarrow CsPbBr_3$ in this context could be caused by a polymer which acts both as a reactant and a macromolecular surfactant,[20] minimizing the number of reagents and preparatory steps involved in the process.

In this work, we demonstrate that poly(maleic anhydride-1-*alt*-octadecene) (PMAO) can simultaneously trigger the $Cs_4PbBr_6 \rightarrow CsPbBr_3$ NC transformation and provide enhanced surface passivation to the resulting $CsPbBr_3$ NCs. PMAO is a widely available co-polymer of 1-octadecene and maleic anhydride and has been extensively used for the surface functionalization of NCs.[22–24] In our experiments, upon mixing PMAO with oleylammonium/oleate-capped Cs_4PbBr_6 NCs, the cyclic anhydride groups of PMAO react with oleylamine species, forming polysuccinamic acid (Fig. 1). Polysuccinamic acid destabilizes the NC surface by displacing both the amine and the oleate ligands and acidifies the reaction environment, thus triggering the formation of $CsPbBr_3$ NCs (Fig. 1). The core chemistry of the NC transformation is summarized by the following chemical equation: Cs_4PbBr_6 + $n$$RNH_2$ + $(-R'(CHCO)_2O-)_n \rightarrow CsPbBr_3 + (-R'(CHCOOH)(CHCONHR)-)_n +$ $3Cs^+_{(solvated)} + 3Br^-_{(solvated)}$, where R = oleyl, R' = octadecenyl,

and the ratio between oleylamine molecules and anhydride units is assumed to be 1 : 1 for simplicity. The extent of the transformation is tunable by varying the amount of added PMAO, enabling the investigation of the transformation intermediates, which consist of Cs_4PbBr_6–$CsPbBr_3$ heterostructures. The fully-transformed $CsPbBr_3$ NCs are bright emitters and retain their green emission for four weeks of storage under ambient conditions in air, even after one washing cycle with ethyl acetate (a solvent which typically causes the degradation of oleylammonium/oleate-capped $CsPbBr_3$ NCs within hours or days). The increase in the stability of $CsPbBr_3$ NCs synthesized from Cs_4PbBr_6 and PMAO is attributed to the adhesion of polysuccinamic acid to the NC surface through its multiple functional groups.

Results and discussion

Cs_4PbBr_6 NCs and their transformation with PMAO in solution

The synthesis of the initial Cs_4PbBr_6 NCs was performed in air, *via* the hot injection of cesium oleate into the solution of lead(II) bromide dissolved in a mixture of oleylamine and oleic acid in 1-octadecene,[7] as detailed in Section S1 of the ESI.† The synthesis is similar to that of $CsPbBr_3$ NCs,[5] except that it is performed at a higher concentration of oleylamine and oleic acid with respect to lead ([oleylamine] : [oleic acid] : [$PbBr_2$] ~0.63 : 0.31 : 0.027 M). Such reaction conditions favor the formation of a Pb-poor Cs_4PbBr_6 phase over the $CsPbBr_3$ phase, as detailed previously.[25] The synthesis delivers batches of Cs-rich rhombohedral Cs_4PbBr_6 NCs with a narrow size distribution and an average diameter in the range from 10 to 16 nm (Fig. 2a, b, and S1–S5†). ^1H and ^1H–^{13}C heteronuclear single quantum coherence (HSQC) nuclear magnetic resonance (NMR) experiments established that Cs_4PbBr_6 NCs are passivated by a mixture of oleylammonium oleate and neutral oleylamine with a ligand ratio of ~3 : 2 between (oleylamine + oleylammonium) : oleate species (see Section S3 and Fig. S6–S9 of the ESI for details†).

These Cs_4PbBr_6 NCs can react with PMAO in toluene, fully or partially transforming into $CsPbBr_3$ NCs, depending on the amount of the added polymer (Fig. 2c). The reaction of Cs_4PbBr_6 NCs with PMAO typically starts within a few minutes after the addition of PMAO at room temperature (Movie S1 and Fig. S10†) and can be accelerated by mild heating of the reaction mixture (up to 80 °C). It is important to highlight here that heating up the NCs alone to 80 °C without the addition of PMAO does not trigger any transformation (Fig. S11†). The fully-transformed $CsPbBr_3$ NCs have a narrow size distribution, as inferred from their self-organization into ordered close-packed monolayers on a carbon-coated TEM copper grid (Fig. 2a). The XRD patterns of the initial NCs, partially- and completely-transformed samples are shown in Fig. 2b. Following the transformation, the XRD reflections of the rhombohedral Cs_4PbBr_6 crystal structure gradually disappeared, and peaks characteristic of the ortho-rhombic $CsPbBr_3$ perovskite phase emerged (Fig. 2b, see Fig. S12† for peak assignment). The progression of the reaction was monitored by steady-state UV-Vis absorption spectroscopy

Fig. 1 Schematic representation of the $Cs_4PbBr_6 \rightarrow CsPbBr_3$ NC transformation induced by PMAO. Oleylamine species from the NC surface react with the cyclic anhydride rings of PMAO, forming polysuccinamic acid. The removal of oleylamine-based and oleate ligands destabilizes the NC surface, and the formation of polysuccinamic acid increases the acidity of the medium, triggering the $Cs_4PbBr_6 \rightarrow CsPbBr_3$ transformation (see the text for the chemical equation). The resulting $CsPbBr_3$ NCs are stabilized by the polysuccinamic acid in place of the original ligands.
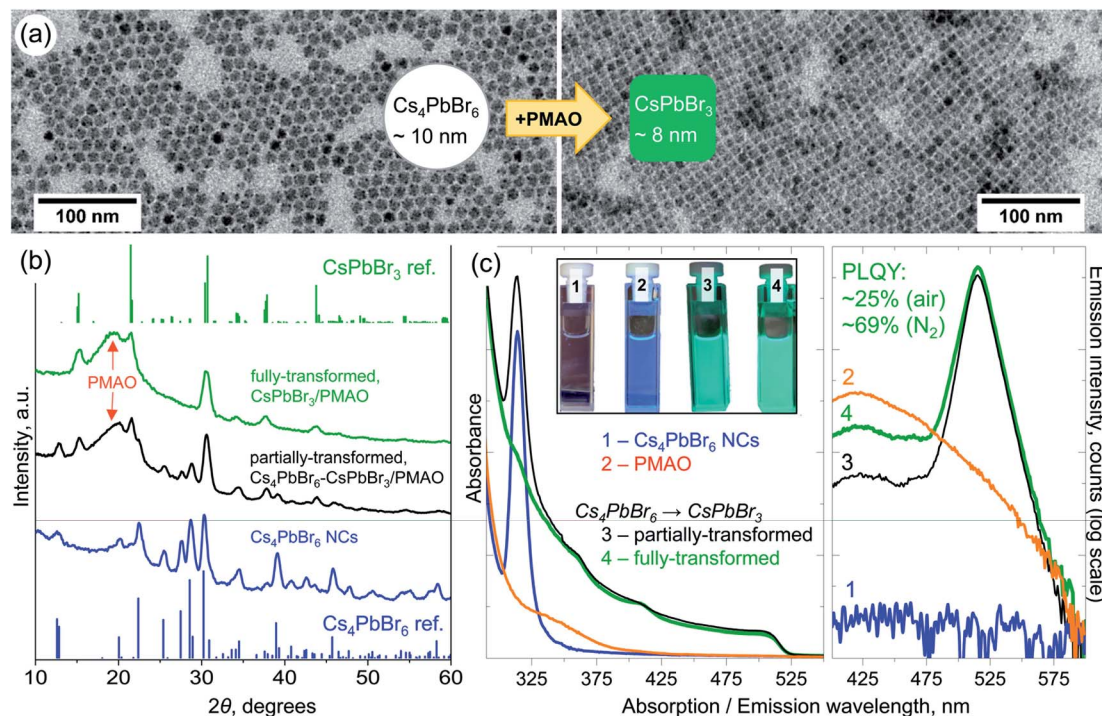
Fig. 2 (a) Low-magnification TEM images of the initial Cs_4PbBr_6 NCs (average diameter 10 ± 1.5 nm) and fully-transformed $CsPbBr_3$ NCs (average edge length 8 ± 0.4 nm) after their reaction with PMAO in toluene. (b) XRD patterns of the initial Cs_4PbBr_6 NCs and of the partially- and fully-transformed ones. Top and bottom stick patterns are those of the reference bulk compounds: rhombohedral Cs_4PbBr_6 (pattern ID 04-015-9683, ICSD code 162158)[27] and orthorhombic $CsPbBr_3$ (pattern ID 96-451-0746, COD code 4510745).[28] The broad peak at ~20° is due to PMAO. (c) Optical absorption (left panel) and emission (right panel) spectra of toluene solutions of initial Cs_4PbBr_6 NCs (blue curve), PMAO (orange curve), and partially- (black curve), and fully-transformed (green curve) NCs. The inset in the left panel shows photographs of the samples under excitation with a 365 nm lamp demonstrating visible green PL of partially- and fully-transformed NC samples.

(Fig. 2c, left panel, Fig. S10†) in which the disappearance of the ~314 nm peak characteristic of Cs_4PbBr_6[7] and the appearance of the ~510 nm band edge absorption of $CsPbBr_3$ are evident. The transformation was also tracked by steady-state photoluminescence (PL) spectroscopy, through the appearance of a cyan emission (λ_{max} ~475–480 nm) in the early stages of the reaction (Fig. S10†). The absolute PL quantum yield (PLQY) of the samples transformed in air was measured to be ~19% (partially transformed), and ~25% (fully transformed). On the other hand, when the transformation was performed under an inert atmosphere, the sample had a 69% PLQY (Fig. S13–S15†). Such a value is comparable to those reported for other Cs_4PbBr_6 → $CsPbBr_3$ chemical transformations of NCs: 47% (ref. 7) and 62% (ref. 11) via the addition of solid $PbBr_2$ at elevated temperatures, and 75% (ref. 12) upon reaction with H_2O. The lower PLQY of the samples transformed in air is attributed to the presence of electron traps formed as a result of sample exposure to atmospheric O_2. Similar results have been reported by Rodà et al. who observed PL dimming in oxygen-exposed $CsPbBr_3$ nanocubes.[26]

Rationalization of the observed reactivity between PMAO and Cs_4PbBr_6 NCs

PMAO is a copolymer of octadecene-1 and maleic anhydride, and it consists of repeating units composed of a saturated hydrocarbon chain and a cyclic succinic anhydride ring (Fig. 1). PMAO has a negligible reactivity towards inorganic salts such as Cs_4PbBr_6, as confirmed in a control experiment on finely ground powder of bulk Cs_4PbBr_6 (Fig. S16 and S17†). However, the succinic anhydride rings of PMAO feature acyl groups that are reactive towards nucleophilic reagents such as water and primary amines (yielding, in the latter case, either succinamic acid at room temperature[23,29–31] or cyclic imides at high temperatures[31–33]). The presence of a significant amount of water as a potential reactant towards PMAO in the Cs_4PbBr_6 NC samples was ruled out based on FTIR and NIR characterization (Fig. S18 and S19†). On the other hand, the ligand shell of Cs_4PbBr_6 NCs contains partially-protonated oleylamine (Section S3 and Fig. S6–S9†). In analogy with the widely studied oleylammonium/oleate-capped $CsPbBr_3$ NCs,[25,34–36] the ligands on the surface of Cs_4PbBr_6 NCs are likely to exist in a dynamic equilibrium between neutral and protonated species (oleylamine and oleylammonium, respectively). Thus neutral oleylamine is always available in the NC solution. Neutral oleylamine is a nucleophile with a documented reactivity towards linear and cyclic anhydrides,[37,38] and polymaleic anhydride derivatives.[39,40] The reaction between neutral oleylamine and PMAO in the absence of NCs causes broadening of the vinyl hydrogen resonance of the oleyl chain in the ^{1}H NMR spectrum due to the attachment of small oleylamine molecules to PMAO

macromolecules (the specified M_w of PMAO is ~30 000–50 000 g mol^{-1}, which roughly corresponds to ~80–150 succinic anhydride-octadecene subunits) (Fig. S20–S22†). The addition of neutral oleylamine to cyclic anhydride produces a succinamic acid derivative, as was confirmed by ^{1}H and ^{1}H–^{13}C HSQC NMR in a control reaction (Fig. S23†). Therefore, the formation of polysuccinamic acid (Fig. 1) is expected upon mixing of PMAO with oleylammonium/oleate capped Cs_4PbBr_6 NCs. The key role of oleylamine species in the $Cs_4PbBr_6 \rightarrow CsPbBr_3$ NC transformation was further verified by a control reaction between PMAO and oleylamine-free Cs_4PbBr_6 NCs (synthesized with tri-n-octylphosphine oxide (TOPO) and oleic acid[41]). The Cs_4PbBr_6 NCs synthesized with TOPO and oleic acid were found to be unreactive towards PMAO (Fig. S27 and S28†).

In summary, the removal of oleylamine from the surface of Cs_4PbBr_6 NCs destabilizes them, while polysuccinamic acid acidifies the reaction environment. Surface destabilization and acidic environments are both general conditions that are known to cause the $Cs_4PbBr_6 \rightarrow CsPbBr_3$ transformation.[10,25,42] The stoichiometry of the transformation is balanced by a nominal removal of 3 equivalents of CsBr from 1 equivalent of Cs_4PbBr_6, yet we have not experimentally detected crystalline CsBr by XRD or high-resolution TEM (HRTEM). This discrepancy is tentatively rationalized by solvation of Cs^+ and Br^- ions by oleate and polysuccinamic acid species, similar to the previously reported dissociation of CsBr in dimethylformamide in the presence of the polyacrylic acid co-polymer.[43] Eventually, our ^{1}H NMR analysis also revealed that the final NCs were capped solely by polysuccinamic acid, indicating the displacement of both the oleate and amine/ammonium ligands from the NC surface

upon transformation (see the discussion in Section S9 and Fig. S20–S26†).

Enhanced stability of the CsPbBr$_3$/PMAO NCs

The fully-transformed $CsPbBr_3$ NCs formed an optically clear solution in toluene. These $CsPbBr_3$ NCs possessed an enhanced stability compared to the polymer-free, ligand-capped $CsPbBr_3$ NCs directly synthesized by following the cesium oleate/lead(II) bromide route.[5,25] Such enhanced stability was demonstrated by the fact that the NCs retained their green emission after four weeks of storage under ambient conditions in air (Fig. S29†), even after undergoing a washing cycle of precipitation/redispersion with ethyl acetate (Fig. S30 and S31†), while the polymer-free $CsPbBr_3$ NCs aggregated within hours or days after undergoing a similar washing procedure. Another indicator of the increased stability is the observation that the $CsPbBr_3$/PMAO NCs could be concentrated or diluted over ~5 orders of magnitude range of concentrations, from ~26 mg ml^{-1} to ~1 × 10^{-4} mg ml^{-1}, without any loss of optical transparency or PL emission (Fig. S32†). The increase in the stability of the fully-transformed $CsPbBr_3$/PMAO NCs is in agreement with prior reports on $CsPbBr_3$ NCs blended with PMAO[44,45] or with the related dodecyl-grafted-poly(isobutylene-alt-maleic-anhydride).[46] Our hypothesis is that the binding of polysuccinamic acid through its multiple functional groups to the NC surface, in place of the standard ligands used in the direct synthesis of $CsPbBr_3$ NCs (as discussed above and in Section S9, Fig. S20–S26†), is the origin of this enhancement. To test this hypothesis, we compared the solvodynamic diameters of PMAO and
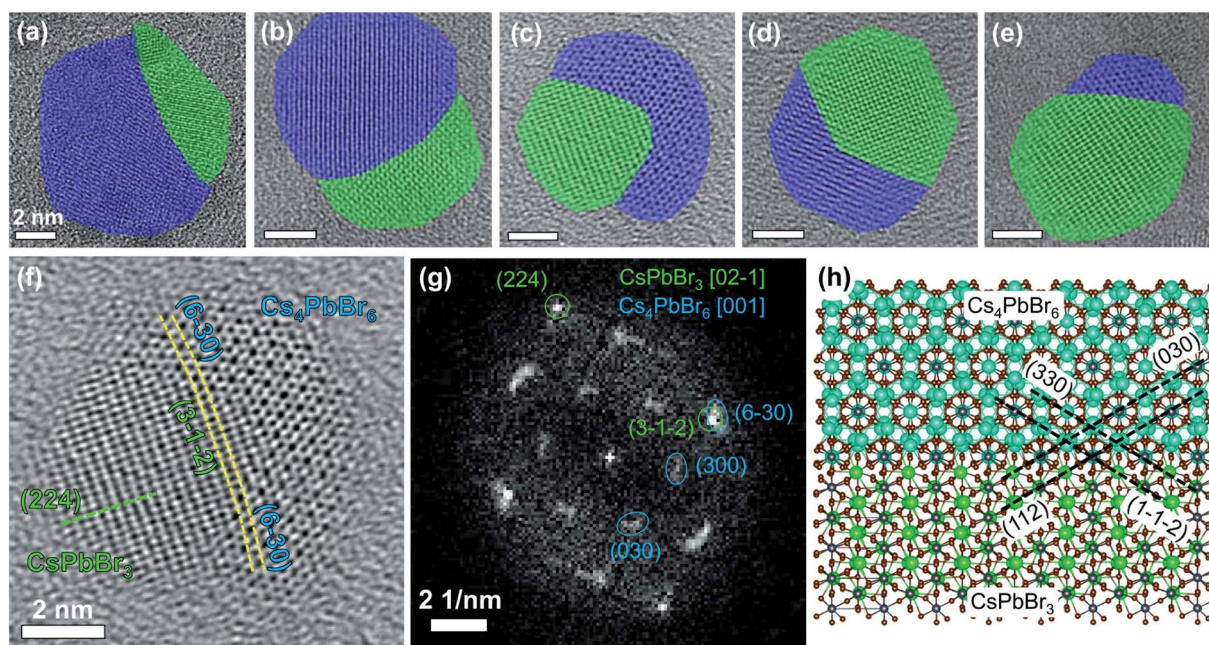

Fig. 3 (a–e) HRTEM images of Cs$_4$PbBr$_6$–CsPbBr$_3$ heterostructures formed upon partial conversion of Cs$_4$PbBr$_6$ NCs with PMAO (scale bars are 2 nm). Cs$_4$PbBr$_6$ domains are shaded in blue, and CsPbBr$_3$ domains are shaded in green; (f) a magnified view of (c) and (g) the corresponding FFT image; and (h) ball-and-stick atomic model of the epitaxial interface built using VESTA software (ver. 3.4.6, the atoms are depicted as spheres with radii corresponding to 40% of actual atomic radii).[47] Cs atoms in the model are colored in two different colors for clarity: in cyan for Cs$_4$PbBr$_6$ and green for CsPbBr$_3$.

$CsPbBr_3$/PMAO NCs (washed once with ethyl acetate) determined by dynamic light scattering (~1.7 ± 1.2 nm and ~11.2 ± 0.9 nm, respectively, Fig. S33 and S34†) with the sizes of the inorganic $CsPbBr_3$ cores from the TEM analysis of the same sample (~7 nm edge length, Fig. S35†). The larger solvodynamic diameter of $CsPbBr_3$/PMAO NCs in solution compared to the $CsPbBr_3$ NC edge length from TEM is explained by the PMAO wrapping and NC tumbling in solution (the diagonal of a cube with a 7 nm edge length is ~12 nm). The lack of a substantial increase in the solvodynamic diameter of $CsPbBr_3$/PMAO NCs is interpreted as an indicator of PMAO wrapping around NCs, supporting the hypothesis about the origin of increased NC stability. In addition, the relatively small solvodynamic diameter of $CsPbBr_3$/PMAO NCs indicates that PMAO molecules do not bind multiple NCs together.

Cs_4PbBr_6–$CsPbBr_3$ heterostructures

The $Cs_4PbBr_6 \rightarrow CsPbBr_3$ NC transformation with PMAO is relatively slow at room temperature. This enabled the observation of NC intermediates consisting of Cs_4PbBr_6–$CsPbBr_3$ heterostructures (Fig. 3), which were investigated by HRTEM (Fig. 3a–e). In one of the partially-transformed samples we observed NCs with different degrees of conversion (Fig. 3a–e). The heterostructures displayed a variety of interfaces between Cs_4PbBr_6 and $CsPbBr_3$, some adopting an epitaxial relationship, some not (analysis of the cases is shown in Fig. S36†). For example, the heterostructure shown in Fig. 3c, analyzed in detail in Fig. 3f–h, is characterized by an epitaxial relationship adopted by the two domains, as indicated by the overlap of the spots from the planes of the two crystal structures in fast Fourier transform (FFT, Fig. 3g) of the real space image. The <5% mismatch between the atomic spacing of the two domains $[d(3\overline{1}2)_{CsPbBr_3} = 2.37$ Å, $d(6\overline{3}0)_{Cs_4PbBr_6} = 2.29$ Å] leads to a slight bending of the planes, as labeled by the dashed lines in Fig. 3f. This bending also indicates that the atomic planes of Cs_4PbBr_6 domains on the two sides of the $CsPbBr_3$ domain are rotated by a small angle. The rotation gives rise to extended diffraction spots in the FFT image, instead of single sharp spots that would otherwise appear for a single crystal. Considering an orthorhombic phase for $CsPbBr_3$ (ICSD: 97851, $a = 8.207$ Å, $b = 8.255$ Å, $c = 11.759$ Å), the epitaxial relationship between the two domains can be described as follows: $CsPbBr_3$ $[02\overline{1}]\|Cs_4PbBr_6$ [001], and $CsPbBr_3$ (112)$\|Cs_4PbBr_6$ (030) (see Fig. 3h).

The low-magnification TEM images of the two NC samples were analyzed to quantify changes in the NC dimensions before and after the transformation (Fig. S37–S42†). For example, a sample of 10.1 nm ± 1.4 nm diameter Cs_4PbBr_6 NCs transformed into 8 nm ± 0.4 nm edge length $CsPbBr_3$ NCs (Fig. 2a). The Scherrer analysis of the XRD patterns of the same sample before and after the transformation indicated a reduction in the crystallite size from 16.1 ± 1.8 nm to 12.5 ± 2.6 nm, in agreement with the TEM analysis (larger dimensions from XRD as compared to TEM are due to the differences between techniques and analyses). In another sample, 15.7 nm ± 2.6 nm Cs_4PbBr_6 NCs transformed into 12 nm ± 1.9 nm NCs (dimensions from TEM). If one assumes that such transformation does

not proceed by dissolution–recrystallization, but simply by the gradual removal of CsBr from each individual spherical NC of Cs_4PbBr_6, converting it to a cube-shaped NC of $CsPbBr_3$, then by volume contraction the resulting $CsPbBr_3$ NCs should have an edge length of 6 nm in TEM (9.5 nm in the second sample), which is ~2 nm smaller than the obtained value (Table S1†). Hence, dissolution–recrystallization processes should also play an important role in this transformation. A similar mechanism has been previously invoked to rationalize the inverse NC transformation (from $CsPbBr_3$ to Cs_4PbBr_6).[8,10]

The PL of the partially-converted sample containing Cs_4PbBr_6–$CsPbBr_3$ heterostructures was surveyed at room and
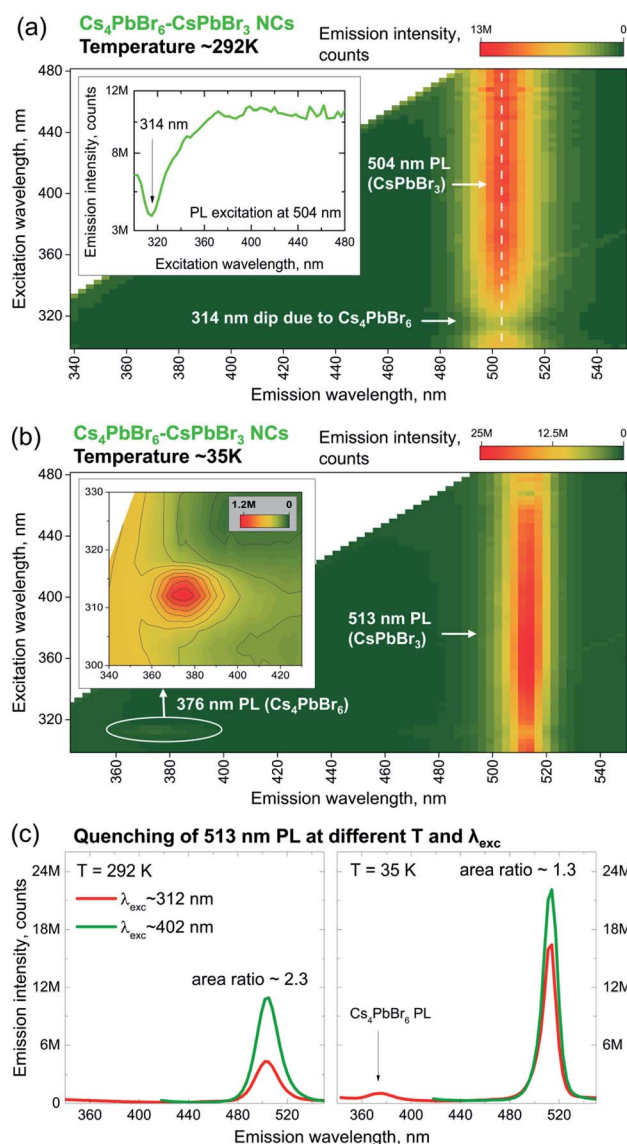

Fig. 4 PL maps of (a) partially-transformed Cs_4PbBr_6–$CsPbBr_3$ NCs at room temperature, and the inset shows the PL excitation spectrum at ~504 nm (indicated by a white dashed line in the PL map); (b) partially-transformed Cs_4PbBr_6–$CsPbBr_3$ NCs at ~35 K, and the inset shows the low intensity region around 376 nm; (c) PL spectra of Cs_4PbBr_6–$CsPbBr_3$ NCs at 292 K (left panel) and 35 K (right panel) collected under ~312 nm (red curve) and ~402 nm (green curve) excitation.

cryogenic temperatures (see Section S14 of the ESI† for experimental details) because their optical properties are unknown to date. The results are presented in Fig. 4a and b as excitation-emission maps (PL maps). The room temperature ($T \sim 292$ K) PL map of the partially-converted sample contains a single emission peak of $CsPbBr_3$ at ~ 504 nm (Fig. 4a). The $CsPbBr_3$ emission has a broad PL excitation spectrum (inset in Fig. 4a) with a dip at ~ 314 nm characteristic of Cs_4PbBr_6 absorption. Upon cooling to $T \sim 35$ K, the PL map shows two emission peaks (Fig. 4b): an intense peak at ~ 513 nm and a weak peak at ~ 376 nm (inset in Fig. 4b). The ~ 513 nm peak is an emission feature of $CsPbBr_3$, red-shifted from ~ 504 nm as a result of cooling.[48,49] The ~ 376 nm emission with narrow excitation at ~ 313 nm is assigned to Cs_4PbBr_6 because it matches with previously reported cryogenic PL spectra of bulk Cs_4PbBr_6 (ref. 50) and Cs_4PbBr_6 aggregates in CsBr.[51] This assignment was further confirmed by collecting the PL map of the as-synthesized Cs_4PbBr_6 NCs at $T \sim 27$ K (Fig. S43†). At 27 K, the emission of the as-synthesized Cs_4PbBr_6 NCs is dominated by a peak at ~ 376 nm surrounded by weaker features due to various electronic transitions in Pb^{2+} ions.[52–54] The as-synthesized Cs_4PbBr_6 NCs are not emissive at room temperature and, besides the discussed ~ 376 nm emission, are non-emissive up to the detection limit of 1600 nm when cooled (Fig. S44†).

The dual emission of partially-transformed NCs provides an opportunity to probe the energy transfer between Cs_4PbBr_6 and $CsPbBr_3$. Fig. 4c shows a comparison between pairs of emission spectra for the partially-converted sample collected at two different temperatures (292 K and 35 K) and two different excitation energies: one matching with Cs_4PbBr_6 absorption ($\lambda_{exc} \sim 312$ nm) and one below it ($\lambda_{exc} \sim 402$ nm, only $CsPbBr_3$ absorbs). At 292 K (Fig. 4c, left panel), only $CsPbBr_3$ emits, regardless of excitation energy, and its emission is quenched by a factor of ~ 2.3 after changing the excitation energy from ~ 402 nm to ~ 312 nm. This quenching is attributed to the attenuation of ~ 312 nm excitation due to absorption by Cs_4PbBr_6 and an excitation-

dependent PL efficiency.[55] At 35 K, both materials emit, and the $CsPbBr_3$ emission is quenched by a smaller factor of ~ 1.3 (Fig. 4c, right panel). We can assign the lower quenching of $CsPbBr_3$ emission at 35 K to the energy transfer from Cs_4PbBr_6, which indeed is favored due to the overlap between the emission of the donor (Cs_4PbBr_6) and the absorption of the acceptor ($CsPbBr_3$). These initial observations make Cs_4PbBr_6–$CsPbBr_3$ NCs a promising platform for future spectroscopic studies of the energy flow between lead halide perovskites and related compounds.

Reactivity of Cs_4PbBr_6 NC samples with PMAO in drop-cast films

The reaction described above can also proceed inside a polymer film (as was confirmed by *in situ* Raman spectroscopy, see Fig. S45†), which makes its investigation relevant for the emerging application of blends between PMAO and oleylammonium/oleate-capped perovskite NCs in light-emitting diodes.[44,45] From this point of view, the Cs_4PbBr_6 to $CsPbBr_3$ transformation is an indicator of amine-anhydride reactivity, and its kinetics can be studied *in situ* by steady-state and time-resolved PL. Fig. 5 shows the results of the *in situ* PL measurements from a macroscopic area (~ 2 mm excitation spot size) of the film made by quick drop-casting of a freshly prepared PMAO–Cs_4PbBr_6 NCs blend. Green PL develops within the first few minutes in the drop-cast film, and reaches a stable intensity and position (~ 510 nm, full width at half maximum of 18 nm) after ~ 2 hours (Fig. 5a and b), indicating the timescale of the complete conversion. Both the PL intensity and the absorbance of the film (at 405 nm, the wavelength of the CW laser used for excitation) increase over the course of the transformation, with a characteristic time constant of about ~ 10 minutes (Fig. 5c). Similar kinetics were obtained by *in situ* micro-PL performed with a confocal fluorescence microscope (Fig. S46†), suggesting that the transformation proceeds uniformly across the blend. The PLQY in the film remains almost constant at $\sim 20\%$
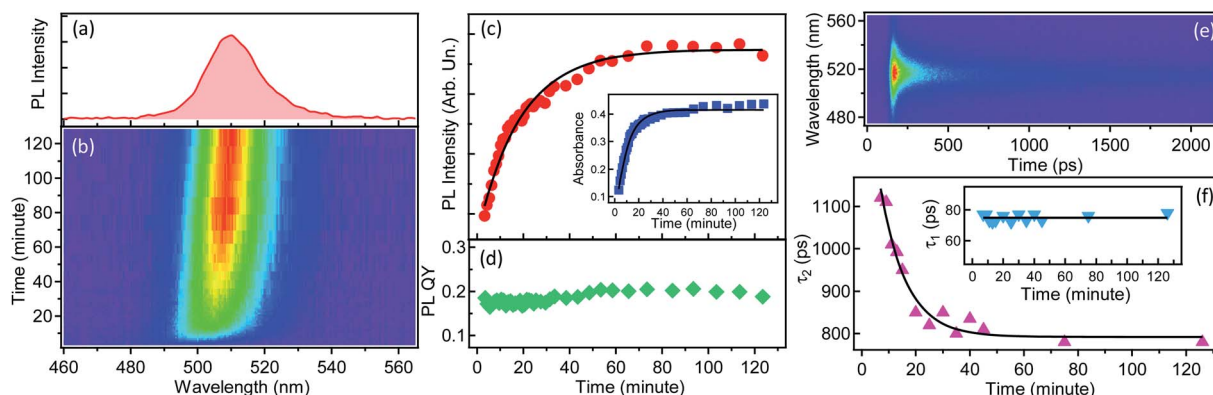

Fig. 5 Tracking the $Cs_4PbBr_6 \rightarrow CsPbBr_3$ NC transformation in a drop-cast film by PL spectroscopy. (a) PL spectrum of the fully transformed $CsPbBr_3$ NCs, peaking at ~ 510 nm. (b) Spectrally-resolved temporal evolution of the PL spectrum on a minute scale, for ~ 120 minutes. (c) Time evolution of the integrated PL intensity fitted with first-order kinetics (solid black line, time ~ 10 min). The inset shows time-dependent absorbance at 405 nm over the course of the transformation. (d) Time-dependent PLQY of the drop-cast film. (e) PL intensity map showing the picosecond temporal behavior of the emission intensity of the drop-cast films. (f) Temporal evolution of the longer PL decay lifetime, τ_2, over the NCs transformation. The continuous line is a fit to the data by first-order kinetics. The corresponding trend for the shorter component, τ_1, is shown in the inset.

throughout the transformation, similar to the values measured in the solution (Fig. 5d).

The evolution of PL during the transformation was also monitored by *in situ* spectrally-resolved transient PL. The temporal PL decay is sub-ns and contains two main components, the shorter ($\sim$70 ps) and longer (950 ps) ones (Fig. 5e and S47†). The shorter decay component varies little over the course of the transformation while the longer decay component decreases from $\sim$1.1 ns to $\sim$800 ps with a time constant of $\sim$10 minutes (Fig. 5f). The PL decay of the emitting NCs in the film is much shorter than that of the NCs in solution ($\sim$4–5 ns), the polymer-free $CsPbBr_3$ NCs[5,35,56–58] ($\sim$2–10 ns), and polymer-encapsulated single $CsPbBr_3$ NCs ($\sim$6 ns).[18] It is definitely much shorter than that of $MAPbBr_3$ NCs/polymer blends (>100 ns).[59] The fast PL decay of $CsPbBr_3$/PMAO NCs in the drop-cast film can be attributed to various possible causes, including: (i) the appearance of a new non-radiative carrier recombination channel, ascribable to oxygen molecules (as the samples were prepared in air) which act as traps for electrons;[26] (ii) electron hopping between neighboring nanocrystals in the film;[60] (iii) a more defective surface of NCs formed in films, due to reduced mobility of ions and molecules (preventing efficient passivation of surface sites in comparison to the solution case). The sub-ns PL decay of NCs in blends with PMAO, combined with a reasonable PLQY, should be of interest for applications in scintillators, where ultrafast and efficient emission is required for fast timing capability of imaging detectors.[61,62]

Conclusions

Chemical transformation of colloidal Cs_4PbBr_6 NCs to perovskite $CsPbBr_3$ NCs induced by the organic co-polymer PMAO is presented as a promising strategy to prepare stable and bright $CsPbBr_3$ NC emitters. The PMAO reactivity towards oleylammonium/oleate-capped Cs_4PbBr_6 NCs favors an addition reaction of oleylamine ligands from the NC surface to the succinic anhydride groups of the polymer. This destabilizes the NCs and acidifies the reaction environment through the formation of polysuccinamic acid, a PMAO–oleylamine adduct, which binds to the surface of the NCs *in lieu* of the original ligands. These two factors – ligand replacement and *in situ* acid formation – drive the Cs_4PbBr_6 to $CsPbBr_3$ NC transformation. The lower reactivity of PMAO, as compared to that of the previously reported reagents, enabled the investigation of Cs_4PbBr_6–$CsPbBr_3$ intermediate heterostructures by HRTEM. The heterostructures feature a variety of epitaxial and non-epitaxial relationships between the two structurally dissimilar domains. At cryogenic temperature, Cs_4PbBr_6–$CsPbBr_3$ NCs display dual emission at $\sim$376 nm and 513 nm with evidence of energy transfer from Cs_4PbBr_6 to $CsPbBr_3$. The PMAO-induced transformation proceeds both in solutions and in drop-cast films, producing $CsPbBr_3$ NCs with a narrow size distribution and attractive photoluminescence properties (up to 69% PLQY in solution and a sub-ns PL lifetime in the drop-cast films). The resulting $CsPbBr_3$/PMAO NCs demonstrate enhanced stability by retaining their green emission for several weeks in air. The increased stability of $CsPbBr_3$/PMAO NCs is attributed to the adhesion of polysuccinamic acid through its multiple functional groups to the NC surface. The PMAO-induced transformation of Cs_4PbBr_6 NCs opens up a general strategy for chemical modification of inorganic NCs passivated with nucleophilic amines.

Author contributions

The manuscript was written through the contributions of all authors. All authors have given approval to the final version of the manuscript.

Conflicts of interest

The authors declare no competing financial interest.

Abbreviations

COD	Crystallography open database
EDS	Energy dispersive X-ray spectroscopy
FFT	Fast Fourier transform
FTIR	Fourier transform infrared spectroscopy
HRTEM	High resolution TEM
HSQC	Heteronuclear single quantum coherence
ICSD	Inorganic crystal structure database
NIR	Near infrared
NMR	Nuclear magnetic resonance
NC	Nanocrystal
PL	Photoluminescence
PMAO	Poly(maleic anhydride-*alt*-1-octadecene)
QY	Quantum yield
STEM	Scanning TEM
TEM	Transmission electron microscopy
XRD	X-ray diffraction

Acknowledgements

"*x*PRINT"), and from MIUR (project "3D-Phys", PRIN 2017PHRM8X).

References

1 M. V. Kovalenko, L. Protesescu and M. I. Bodnarchuk, Properties and potential optoelectronic applications of lead halide perovskite nanocrystals, *Science*, 2017, **358**(6364), 745–750.

2 Q. A. Akkerman, G. Rainò, M. V. Kovalenko and L. Manna, Genesis, challenges and opportunities for colloidal lead halide perovskite nanocrystals, *Nat. Mater.*, 2018, **17**(5), 394–405.

3 J. Shamsi, A. S. Urban, M. Imran, L. De Trizio and L. Manna, Metal Halide Perovskite Nanocrystals: Synthesis, Post-Synthesis Modifications, and Their Optical Properties, *Chem. Rev.*, 2019, **119**(5), 3296–3348.

4 G. Nedelcu, L. Protesescu, S. Yakunin, M. I. Bodnarchuk, M. J. Grotevent and M. V. Kovalenko, Fast Anion-Exchange in Highly Luminescent Nanocrystals of Cesium Lead Halide Perovskites (CsPbX$_3$, X = Cl, Br, I), *Nano Lett.*, 2015, **15**(8), 5635–5640.

5 L. Protesescu, S. Yakunin, M. I. Bodnarchuk, F. Krieg, R. Caputo, C. H. Hendon, R. X. Yang, A. Walsh and M. V. Kovalenko, Nanocrystals of Cesium Lead Halide Perovskites (CsPbX$_3$, X = Cl, Br, and I): Novel Optoelectronic Materials Showing Bright Emission with Wide Color Gamut, *Nano Lett.*, 2015, **15**(6), 3692–3696.

6 Q. A. Akkerman, V. D'Innocenzo, S. Accornero, A. Scarpellini, A. Petrozza, M. Prato and L. Manna, Tuning the Optical Properties of Cesium Lead Halide Perovskite Nanocrystals by Anion Exchange Reactions, *J. Am. Chem. Soc.*, 2015, **137**(32), 10276–10281.

7 Q. A. Akkerman, S. Park, E. Radicchi, F. Nunzi, E. Mosconi, F. De Angelis, R. Brescia, P. Rastogi, M. Prato and L. Manna, Nearly Monodisperse Insulator Cs$_4$PbX$_6$ (X = Cl, Br, I) Nanocrystals, Their Mixed Halide Compositions, and Their Transformation into CsPbX$_3$ Nanocrystals, *Nano Lett.*, 2017, **17**(3), 1924–1930.

8 Z. Liu, Y. Bekenstein, X. Ye, S. C. Nguyen, J. Swabeck, D. Zhang, S.-T. Lee, P. Yang, W. Ma and A. P. Alivisatos, Ligand Mediated Transformation of Cesium Lead Bromide Perovskite Nanocrystals to Lead Depleted Cs$_4$PbBr$_6$ Nanocrystals, *J. Am. Chem. Soc.*, 2017, **139**(15), 5309–5312.

9 F. Palazon, C. Urso, L. De Trizio, Q. Akkerman, S. Marras, F. Locardi, I. Nelli, M. Ferretti, M. Prato and L. Manna, Postsynthesis Transformation of Insulating Cs$_4$PbBr$_6$ Nanocrystals into Bright Perovskite CsPbBr$_3$ through Physical and Chemical Extraction of CsBr, *ACS Energy Lett.*, 2017, **2**(10), 2445–2448.

10 T. Udayabhaskararao, L. Houben, H. Cohen, M. Menahem, I. Pinkas, L. Avram, T. Wolf, A. Teitelboim, M. Leskes, O. Yaffe, D. Oron and M. Kazes, A Mechanistic Study of Phase Transformation in Perovskite Nanocrystals Driven by Ligand Passivation, *Chem. Mater.*, 2018, **30**(1), 84–93.

11 Y. Li, H. Huang, Y. Xiong, S. V. Kershaw and A. L. Rogach, Reversible transformation between CsPbBr$_3$ and

12 L. Wu, H. Hu, Y. Xu, S. Jiang, M. Chen, Q. Zhong, D. Yang, Q. Liu, Y. Zhao, B. Sun, Q. Zhang and Y. Yin, From Nonluminescent Cs$_4$PbX$_6$ (X = Cl, Br, I) Nanocrystals to Highly Luminescent CsPbX$_3$ Nanocrystals: Water-Triggered Transformation through a CsX-Stripping Mechanism, *Nano Lett.*, 2017, **17**(9), 5799–5804.

13 H. Hu, L. Wu, Y. Tan, Q. Zhong, M. Chen, Y. Qiu, D. Yang, B. Sun, Q. Zhang and Y. Yin, Interfacial Synthesis of Highly Stable CsPbX$_3$/Oxide Janus Nanoparticles, *J. Am. Chem. Soc.*, 2018, **140**(1), 406–412.

14 L. Yang, T. Wang, Q. Min, B. Liu, Z. Liu, X. Fan, J. Qiu, X. Xu, J. Yu and X. Yu, High Water Resistance of Monoclinic CsPbBr$_3$ Nanocrystals Derived from Zero-Dimensional Cesium Lead Halide Perovskites, *ACS Omega*, 2019, **4**(3), 6084–6091.

15 M. Chen, H. Hu, Y. Tan, N. Yao, Q. Zhong, B. Sun, M. Cao, Q. Zhang and Y. Yin, Controlled growth of dodecapod-branched CsPbBr$_3$ nanocrystals and their application in white light emitting diodes, *Nano Energy*, 2018, **53**, 559–566.

16 Y. Wei, Z. Cheng and J. Lin, An overview on enhancing the stability of lead halide perovskite quantum dots and their applications in phosphor-converted LEDs, *Chem. Soc. Rev.*, 2019, **48**(1), 310–350.

17 S. N. Raja, Y. Bekenstein, M. A. Koc, S. Fischer, D. Zhang, L. Lin, R. O. Ritchie, P. Yang and A. P. Alivisatos, Encapsulation of Perovskite Nanocrystals into Macroscale Polymer Matrices: Enhanced Stability and Polarization, *ACS Appl. Mater. Interfaces*, 2016, **8**(51), 35523–35533.

18 G. Rainò, A. Landuyt, F. Krieg, C. Bernasconi, S. T. Ochsenbein, D. N. Dirin, M. I. Bodnarchuk and M. V. Kovalenko, Underestimated Effect of a Polymer Matrix on the Light Emission of Single CsPbBr$_3$ Nanocrystals, *Nano Lett.*, 2019, **19**(6), 3648–3653.

19 Y. Wang, Y. Zhu, J. Huang, J. Cai, J. Zhu, X. Yang, J. Shen, H. Jiang and C. Li, CsPbBr$_3$ Perovskite Quantum Dots-Based Monolithic Electrospun Fiber Membrane as an Ultrastable and Ultrasensitive Fluorescent Sensor in Aqueous Medium, *J. Phys. Chem. Lett.*, 2016, **7**(21), 4253–4258.

20 H. Kim, S. So, A. Ribbe, Y. Liu, W. Hu, V. V. Duzhko, R. C. Hayward and T. Emrick, Functional polymers for growth and stabilization of CsPbBr$_3$ perovskite nanoparticles, *Chem. Commun.*, 2019, **55**(12), 1833–1836.

21 H. Kim, N. Hight-Huf, J.-H. Kang, P. Bisnoff, S. Sundararajan, T. Thompson, M. Barnes, R. Hayward and T. S. Emrick, Polymer Zwitterions for Stabilization of CsPbBr$_3$ Perovskite Nanoparticle and Nanocomposite Films, *Angew. Chem., Int. Ed.*, DOI: 10.1002/anie.201916492, accepted article.

22 T. Pellegrino, L. Manna, S. Kudera, T. Liedl, D. Koktysh, A. L. Rogach, S. Keller, J. Rädler, G. Natile and W. J. Parak, Hydrophobic Nanocrystals Coated with an Amphiphilic Polymer Shell: A General Route to Water Soluble Nanocrystals, *Nano Lett.*, 2004, **4**(4), 703–707.

23 C.-A. J. Lin, R. A. Sperling, J. K. Li, T.-Y. Yang, P.-Y. Li, M. Zanella, W. H. Chang and W. J. Parak, Design of an Amphiphilic Polymer for Nanoparticle Coating and Functionalization, *Small*, 2008, **4**(3), 334–341.

24 R. Di Corato, A. Quarta, P. Piacenza, A. Ragusa, A. Figuerola, R. Buonsanti, R. Cingolani, L. Manna and T. Pellegrino, Water solubilization of hydrophobic nanocrystals by means of poly(maleic anhydride-*alt*-1-octadecene), *J. Mater. Chem.*, 2008, **18**(17), 1991–1996.

25 G. Almeida, L. Goldoni, Q. Akkerman, Z. Dang, A. H. Khan, S. Marras, I. Moreels and L. Manna, Role of Acid–Base Equilibria in the Size, Shape, and Phase Control of Cesium Lead Bromide Nanocrystals, *ACS Nano*, 2018, **12**(2), 1704–1711.

26 C. Rodà, A. L. Abdelhady, J. Shamsi, M. Lorenzon, V. Pinchetti, M. Gandini, F. Meinardi, L. Manna and S. Brovelli, O_2 as a molecular probe for nonradiative surface defects in $CsPbBr_3$ perovskite nanostructures and single crystals, *Nanoscale*, 2019, **11**(16), 7613–7623.

27 M. Velázquez, A. Ferrier, S. Péchev, P. Gravereau, J.-P. Chaminade, X. Portier and R. Moncorgé, Growth and characterization of pure and Pr^{3+}-doped Cs_4PbBr_6 crystals, *J. Cryst. Growth*, 2008, **310**(24), 5458–5463.

28 C. C. Stoumpos, C. D. Malliakas, J. A. Peters, Z. Liu, M. Sebastian, J. Im, T. C. Chasapis, A. C. Wibowo, D. Y. Chung, A. J. Freeman, B. W. Wessels and M. G. Kanatzidis, Crystal Growth of the Perovskite Semiconductor $CsPbBr_3$: A New Material for High-Energy Radiation Detection, *Cryst. Growth Des.*, 2013, **13**(7), 2722–2727.

29 R. Kluger and J. C. Hunt, Aminolysis of maleic anhydride. Kinetics and thermodynamics of amide formation, *J. Am. Chem. Soc.*, 1984, **106**(19), 5667–5670.

30 R. Kluger and J. C. Hunt, Circumventive catalysis: contrasting reaction patterns of tertiary and primary amines with cyclic anhydrides and the avoidance of intermediates, *J. Am. Chem. Soc.*, 1989, **111**(9), 3325–3328.

31 Z. Jin, L. Du, C. Zhang, Y. Sugiyama, W. Wang, G. Palui, S. Wang and H. Mattoussi, Modification of Poly(maleic anhydride)-Based Polymers with $H_2N–R$ Nucleophiles: Addition or Substitution Reaction?, *Bioconjugate Chem.*, 2019, **30**(3), 871–880.

32 L. Coleman, J. Bork and H. Dunn, Notes. Reaction of Primary Aliphatic Amines with Maleic Anhydride, *J. Org. Chem.*, 1959, **24**(1), 135–136.

33 I. Vermeesch and G. Groeninckx, Chemical modification of poly(styrene-co-maleic anhydride) with primary N-alkylamines by reactive extrusion, *J. Appl. Polym. Sci.*, 1994, **53**(10), 1365–1373.

34 J. De Roo, M. Ibáñez, P. Geiregat, G. Nedelcu, W. Walravens, J. Maes, J. C. Martins, I. Van Driessche, M. V. Kovalenko and Z. Hens, Highly Dynamic Ligand Binding and Light Absorption Coefficient of Cesium Lead Bromide Perovskite Nanocrystals, *ACS Nano*, 2016, **10**(2), 2071–2081.

35 M. I. Bodnarchuk, S. C. Boehme, S. ten Brinck, C. Bernasconi, Y. Shynkarenko, F. Krieg, R. Widmer, B. Aeschlimann, D. Günther, M. V. Kovalenko and I. Infante, Rationalizing and Controlling the Surface Structure and Electronic Passivation of Cesium Lead Halide Nanocrystals, *ACS Energy Lett.*, 2019, **4**(1), 63–74.

36 D. Quarta, M. Imran, A.-L. Capodilupo, U. Petralanda, B. van Beek, F. De Angelis, L. Manna, I. Infante, L. De Trizio and C. Giansante, Stable Ligand Coordination at the Surface of Colloidal $CsPbBr_3$ Nanocrystals, *J. Phys. Chem. Lett.*, 2019, **10**(13), 3715–3726.

37 S. Watanabe, H. Kawahara and T. Kuramochi, Adducts of cyclic acid anhydrides and fatty amines as anti-rust additives in water-based cutting fluids, *J. Am. Oil Chem. Soc.*, 1991, **68**(2), 92–94.

38 M. Abbas and C. Slugovc, Optimized reaction conditions for the cross-metathesis of methyl oleate and oleylamine with ethyl acrylate, *Monatsh. Chem.*, 2012, **143**(4), 669–673.

39 S. Percec, L. Howe, J. Li and S. Bair, Chemical modification of poly(ethylene-co-methyl acrylate-co-maleic anhydride) for cathodic electrodepositions, *J. Polym. Sci., Part A: Polym. Chem.*, 2012, **50**(2), 261–270.

40 C. Zhang, C. Gao, F. Gao, J. Wang, D. Zhang, Y. Wang and D. Xu, Synthesis of comb bipolymers and their pour point depressing properties, *Pet. Sci.*, 2014, **11**(1), 155–160.

41 G. Almeida, O. J. Ashton, L. Goldoni, D. Maggioni, U. Petralanda, N. Mishra, Q. A. Akkerman, I. Infante, H. J. Snaith and L. Manna, The Phosphine Oxide Route toward Lead Halide Perovskite Nanocrystals, *J. Am. Chem. Soc.*, 2018, **140**(44), 14878–14886.

42 S. Park, N. M. An, G. Almeida, F. Palazon, D. Spirito, R. Krahne, Z. Dang, L. De Trizio and L. Manna, $CsPbX_3/SiO_x$ (X=Cl, Br, I) Monoliths Prepared via a Novel Sol-gel Route Starting from Cs_4PbX_6 Nanocrystals, *Nanoscale*, 2019, **11**(40), 18739–18745.

43 Y. Liu, Z. Wang, S. Liang, Z. Li, M. Zhang, H. Li and Z. Lin, Polar Organic Solvent-Tolerant Perovskite Nanocrystals Permanently Ligated with Polymer Hairs via Star-like Molecular Bottlebrush Trilobe Nanoreactors, *Nano Lett.*, 2019, **19**(12), 9019–9028.

44 M. Meyns, M. Perálvarez, A. Heuer-Jungemann, W. Hertog, M. Ibáñez, R. Nafria, A. Genç, J. Arbiol, M. V. Kovalenko, J. Carreras, A. Cabot and A. G. Kanaras, Polymer-Enhanced Stability of Inorganic Perovskite Nanocrystals and Their Application in Color Conversion LEDs, *ACS Appl. Mater. Interfaces*, 2016, **8**(30), 19579–19586.

45 H. Wu, S. Wang, F. Cao, J. Zhou, Q. Wu, H. Wang, X. Li, L. Yin and X. Yang, Ultrastable Inorganic Perovskite Nanocrystals Coated with a Thick Long-Chain Polymer for Efficient White Light-Emitting Diodes, *Chem. Mater.*, 2019, **31**(6), 1936–1940.

46 C. Carrillo-Carrión, P. del Pino and B. Pelaz, Aqueous stable luminescent perovskite-polymer composites, *Applied Materials Today*, 2019, **15**, 562–569.

47 K. Momma and F. Izumi, VESTA 3 for three-dimensional visualization of crystal, volumetric and morphology data, *J. Appl. Crystallogr.*, 2011, **44**(6), 1272–1276.

48 A. D. Wright, C. Verdi, R. L. Milot, G. E. Eperon, M. A. Pérez-Osorio, H. J. Snaith, F. Giustino, M. B. Johnston and

L. M. Herz, Electron–phonon coupling in hybrid lead halide perovskites, *Nat. Commun.*, 2016, **7**(1), 11755.

49 Y. Guo, O. Yaffe, T. D. Hull, J. S. Owen, D. R. Reichman and L. E. Brus, Dynamic emission Stokes shift and liquid-like dielectric solvation of band edge carriers in lead-halide perovskites, *Nat. Commun.*, 2019, **10**(1), 1175.

50 M. Nikl, E. Mihokova, K. Nitsch, F. Somma, C. Giampaolo, G. P. Pazzi, P. Fabeni and S. Zazubovich, Photoluminescence of Cs_4PbBr_6 crystals and thin films, *Chem. Phys. Lett.*, 1999, **306**(5), 280–284.

51 V. Babin, P. Fabeni, E. Mihokova, M. Nikl, G. P. Pazzi, N. Zazubovich and S. Zazubovich, Luminescence of Cs_4PbBr_6 Aggregates in As-Grown and in Annealed CsBr:Pb Single Crystals, *Phys. Status Solidi B*, 2000, **219**(1), 205–214.

52 S. Radhakrishna and K. P. Pande, Lead Centers in Cesium Halides, *Phys. Rev. B*, 1973, **7**(1), 424–431.

53 P. W. M. Jacobs, Alkali halide crystals containing impurity ions with the ns^2 ground-state electronic configuration, *J. Phys. Chem. Solids*, 1991, **52**(1), 35–67.

54 J. Yin, Y. Zhang, A. Bruno, C. Soci, O. M. Bakr, J.-L. Brédas and O. F. Mohammed, Intrinsic Lead Ion Emissions in Zero-Dimensional Cs_4PbBr_6 Nanocrystals, *ACS Energy Lett.*, 2017, **2**(12), 2805–2811.

55 J. Hoy, P. J. Morrison, L. K. Steinberg, W. E. Buhro and R. A. Loomis, Excitation Energy Dependence of the Photoluminescence Quantum Yields of Core and Core/ Shell Quantum Dots, *J. Phys. Chem. Lett.*, 2013, **4**(12), 2053–2060.

56 M. Imran, V. Caligiuri, M. Wang, L. Goldoni, M. Prato, R. Krahne, L. De Trizio and L. Manna, Benzoyl Halides as Alternative Precursors for the Colloidal Synthesis of Lead-Based Halide Perovskite Nanocrystals, *J. Am. Chem. Soc.*, 2018, **140**(7), 2656–2664.

57 M. Imran, P. Ijaz, D. Baranov, L. Goldoni, U. Petralanda, Q. Akkerman, A. L. Abdelhady, M. Prato, P. Bianchini, I. Infante and L. Manna, Shape-Pure, Nearly Monodispersed $CsPbBr_3$ Nanocubes Prepared Using Secondary Aliphatic Amines, *Nano Lett.*, 2018, **18**(12), 7822–7831.

58 M. Imran, P. Ijaz, L. Goldoni, D. Maggioni, U. Petralanda, M. Prato, G. Almeida, I. Infante and L. Manna, Simultaneous Cationic and Anionic Ligand Exchange For Colloidally Stable $CsPbBr_3$ Nanocrystals, *ACS Energy Lett.*, 2019, **4**(4), 819–824.

59 Y. Wang, J. He, H. Chen, J. Chen, R. Zhu, P. Ma, A. Towers, Y. Lin, A. J. Gesquiere, S.-T. Wu and Y. Dong, Ultrastable, Highly Luminescent Organic–Inorganic Perovskite–Polymer Composite Films, *Adv. Mater.*, 2016, **28**(48), 10710–10717.

60 S. J. Yoon, Z. Guo, P. C. dos Santos Claro, E. V. Shevchenko and L. Huang, Direct Imaging of Long-Range Exciton Transport in Quantum Dot Superlattices by Ultrafast Microscopy, *ACS Nano*, 2016, **10**(7), 7208–7215.

61 C. Dujardin, E. Auffray, E. Bourret-Courchesne, P. Dorenbos, P. Lecoq, M. Nikl, A. N. Vasil'ev, A. Yoshikawa and R. Zhu, Needs, Trends, and Advances in Inorganic Scintillators, *IEEE Trans. Nucl. Sci.*, 2018, **65**(8), 1977–1997.

62 K. Tomanová, V. Čuba, M. G. Brik, E. Mihóková, R. M. Turtos, P. Lecoq, E. Auffray and M. Nikl, On the structure, synthesis, and characterization of ultrafast blue-emitting $CsPbBr_3$ nanoplatelets, *APL Mater.*, 2019, **7**(1), 011104.